

Article

Structural Effects of Residual Groups of Graphene Oxide on Poly(ϵ -Caprolactone)/Graphene Oxide Nanocomposite

Tianchen Duan ¹, You Lv ¹, Haojun Xu ¹, Jing Jin ² and Zongbao Wang ^{1,*}

¹ Ningbo Key Laboratory of Specialty Polymers, Faculty of Materials Science and Chemical Engineering, Ningbo University, Ningbo 315211, China; duantianchen@foxmail.com (T.D.); lvyou725@163.com (Y.L.); xuhaojun_nbu@163.com (H.X.)

² State Key Laboratory of Polymer Physics and Chemistry, Changchun Institute of Applied Chemistry, Chinese Academy of Sciences, Changchun 130022, China; jjin@ciac.ac.cn

* Correspondence: wangzongbao@nbu.edu.cn; Tel.: +86-0574-8760-0734

Received: 31 May 2018; Accepted: 22 June 2018; Published: 28 June 2018



Abstract: In this work, the crystallization behaviors, such as degree of crystallinity and crystalline thickness of poly(ϵ -caprolactone) (PCL) matrix with the incorporation of graphene oxide (GO) and their evolution with time were examined in order to better understand the influences of residual groups of GO on the semi-crystalline polyester. The results showed that the residual strong oxidizing debris on the GO surface could induce the degradation of amorphous parts in PCL matrix. Moreover, the increasing degree of crystallinity and almost constant crystalline thickness implies that oxidative degradation cannot degrade the crystal structure of PCL matrix.

Keywords: poly(ϵ -caprolactone); graphene oxide; structural evolution; residual group

1. Introduction

Graphene oxide (GO) sheets are atomically thick, two-dimensional (2D) layered materials, and are important members of the graphene-based materials. The same as graphene, GO also has excellent mechanical, thermal and electrical properties [1,2]. The traditional route to synthesize GO involves two steps: oxidation of graphite powder by the Hummers [3] or Staudenmaier [4] method, and exfoliation of graphite oxide. The oxidation process needs strong oxidizing agents such as sulfuric acid, potassium chlorate, potassium nitrate, potassium permanganate and nitric acid. The introduction of oxygen-containing groups (such as hydroxyl, epoxy, carbonyl and carboxyl groups) [5] can increase the hydrophilic ability of GO. With large content of functional groups, GO could form stable single-layer suspensions in water or other common polar solvents [6].

The above unique properties promise a wide variety of applications for GO. The incorporation of GO into polymers has drawn much attention as a route to obtain new materials with excellent properties. As a nano-scale material, 2D layered GO can affect the crystallization behaviors of semi-crystalline polymers. Xu et al. investigated the isothermal and nonisothermal crystallization of isotactic polypropylene (iPP)/GO nanocomposites. They reported that the incorporation of GO can enhance the formation of long ordering segment in iPP crystallization process [7,8]. Huang et al. reported that GO could have a twofold effect on the poly(L-lactic acid) (PLLA) crystallization process: as heterogeneous nucleation agent and for space confinement [9]. Wang et al. prepared poly(ϵ -caprolactone) (PCL)/GO nanocomposites by in situ polymerization, and Hua et al. used a ring-opening polymerization method, finding that GO could act as a nucleation agent to enhance the crystallization of PCL in the nanocomposites [10,11]. Moreover, with excellent mechanical properties and large aspect ratio, GO can improve the mechanical properties of polymer matrix. Previous studies

indicated that GO can enhance the mechanical properties of PCL matrix [12,13]. It has also been used to reinforce other polymer matrices, such as natural rubber [14], poly(arylene ether nitrile) [15], poly(vinyl chloride) [16], epoxy [17], silicone [18], polyurethane [19], poly(butylene succinate) [20], elastomer [21] and PP [22].

Additionally, the functional groups on the GO surface could have strong interactions with the polar groups in certain polymer matrices. Hua et al. modified the surface of GO with octyltrichlorosilane and found that PCL/GO nanocomposites exhibited improvements in the mechanical, electrical conductivity properties and crystallization behaviors compared with Neat PCL [23]. Cai et al. confirmed that thermal treatment was an effective approach to create a polymer crystalline layer on the surface of GO in PCL melts; a non-covalent interface for stress transfer can be enhanced by this polymer crystalline layer [24]. Li et al. firstly used Raman spectroscopy to investigate the interfacial stress transfer in poly(vinyl alcohol) (PVA)/GO nanocomposites [25]. Valles et al. reported that the presence of the oxidative debris on GO surface could act as compatibilizing surfactants, which was beneficial in producing poly(methyl methacrylate) (PMMA)/GO nanocomposites with good dispersion and strong interface [26]. Zhao et al. fabricated ultrathin multilayer PVA/GO films by a bottom-up layer-by-layer assembly technique, and a significant enhancement of mechanical properties was achieved [27]. Wan et al. studied the interfacial interaction between GO and polymer matrices such as PLLA, PCL, polystyrene (PS) and high-density polyethylene (HDPE). They reported that GO could uniformly disperse in the polar polymer (PCL and PLLA) and had strong interaction with the polymer matrix [28].

The structure and mechanical properties of polymer/GO nanocomposites have been widely studied, and the interactions of functional groups on GO surface with the polar groups in polymer matrix have been studied, but the structural evolution with time and the effects of residual groups of GO surface on polymer/GO nanocomposites have rarely been investigated. PCL, as an aliphatic polyester exhibiting excellent biocompatibility [29] and biodegradability [30], has been widely used in many fields. In this work, PCL was chosen as a model polymer of semi-crystalline polyester to investigate the structural evolution of polyester/GO nanocomposites. PCL/GO nanocomposites with different contents of residual groups were prepared by changing the content of GO in the nanocomposites. The crystallization behaviors, such as degree of crystallinity and crystalline thickness of PCL matrix with the incorporation of GO and their evolution with time were examined in order to better understand the influences of residual groups of GO on the semi-crystalline polyester.

2. Materials and Methods

2.1. Materials

PCL was purchased from Shanghai Yizhu Co., Ltd. (Shanghai, China), with average weight $M_n = 35,000 \text{ g}\cdot\text{mol}^{-1}$. Natural flake graphite was purchased from Qingdao Jiuyi graphite Co., Ltd. (Shandong, China) with mean particle size of 50 μm . Sulfuric acid (H_2SO_4) (98%), potassium peroxydisulfate ($\text{K}_2\text{S}_2\text{O}_8$), phosphoric anhydride (P_2O_5), potassium permanganate (KMnO_4), hydrogen peroxide (H_2O_2) (35%), hydrochloric (HCl) (37%), ethanol and chloroform were purchased from Sinopharm Chemical Reagent Co., Ltd. (Shanghai, China). All reagents were used as received without further purification.

2.2. Sample Preparation

GO was exfoliated by ultra-sonication from graphite oxide which was produced by modified Hummers' method [31–33]. PCL/GO nanocomposites with various GO concentrations of 0.1, 0.5 and 1.0 wt.% were prepared by solution coagulation method. Firstly, GO was added to ethanol by ultra-sonication for 1h and PCL was completely dissolved in chloroform. By dropping the pre-dispersed ethanol/GO suspension into the chloroform/PCL mixture, PCL/GO nanocomposites were precipitated. The obtained nanocomposites were dried in vacuum at 50 °C for 2 days to remove the solvent completely. Neat PCL was prepared with the same procedure in order to eliminate

experimental error. Finally, the standard bars were prepared by HAAKE MiniJet II micro-injection molding machine. The melt temperature, mold temperature and injection pressure were preset at 90 °C, 30 °C and 650 bar, respectively. All samples were kept in a desiccator containing allochroic silicagel at room temperature. For brevity, they were abbreviated as Neat PCL, PCL/GO-0.1, PCL/GO-0.5 and PCL/GO-1.0, respectively, in this work from now on.

2.3. Analytical Methods

Two-dimensional small-angle X-ray scattering (2D-SAXS) experiments and two-dimensional wide-angle X-ray diffraction (2D-WAXD) experiments were carried out on the BL16B1 beam-line in the Shanghai Synchrotron Radiation Facility (SSRF). The 2D patterns were recorded in transmission mode at room temperature, the sample-to-detector distance was 2000 mm for SAXS and 169 mm for WAXD. The wavelength of the monochromatic X-ray was 1.24 Å. SAXS and WAXD curves were collected from the 2D patterns. Differential scanning calorimetry (DSC) measurements were performed with Mettler Toledo DSC under nitrogen atmosphere. All samples were first heated to 90 °C at a heating rate of 10 °C/min, and equilibrated at 90 °C for 3 min to remove thermal history. Subsequently, the samples were cooled to −10 °C at a cooling rate of 10 °C/min (cooling curve). At last, all samples were reheated to 90 °C at a heating rate of 10 °C/min (second heating curve). Gel permeation chromatography (GPC) measurements were performed by Waters 2414 GPC. Chloroform was used as a mobile phase and polystyrene solution was used as the calibration standard. M_n , M_w , and PDI of PCL were calculated with the Maxima 820 software. For PCL/GO nanocomposites, GO was separated by filtering the solutions before the measurements. X-ray photoelectron spectroscopy (XPS) experiments were carried out using AXIS UTLTRADLD, operated at 15 kV under a current of 30 mA.

3. Results and Discussion

With a 2D nano-layered structure, GO can influence the crystallization behaviors of polymer matrix. 2D-SAXS was used to investigate the influences of GO on the long period, orientation of PCL matrix and their evolution with time. Figure 1 shows the 2D-SAXS patterns of PCL and its nanocomposites after being kept for 5 (a–d) and 50 (e–h) days after preparation. As shown in Figure 1a–d, neat PCL and its nanocomposites show an isotropic reflection circle with two small scattering spots in the flow direction. For PCL/GO nanocomposites, the scattering signals gather on scattering spots with the increase of GO content. Previous research confirmed that 2D-layered nanofiller could enhance the orientation of polymer chains [12,34]. Thus, the gathering of the scattering signals can be attributed to GO layers that could restrict the mobility of oriented PCL chains; this is similar to the explanation proposed in polyester/GO nanocomposites [9,35]. The 2D-SAXS patterns of neat PCL and its nanocomposites after 50 days show notable changes (Figure 1e–h). Firstly, the diameter of the reflection circle gradually increases with increasing GO content, especially for PCL/GO-0.5 and PCL/GO-1.0, which means that the long period of PCL matrix is affected by the GO content and storage time. Secondly, the scattering spots disappear from PCL/GO nanocomposites after leaving 50 days, which implies that the orientation of PCL matrix has been weakened in the storage process.

SAXS intensity profiles of all samples are further presented in order to investigate the structural changes of PCL matrix. Figure 2 shows the radially integrated profiles (flow direction) of neat PCL and its nanocomposites after leaving 50 days. The long period of PCL matrix can be calculated through the Bragg equation, $L = 2\pi/q^*$, where L is long period, and q^* represents the peak position in the $I-q$ curves. As shown in Figure 2, the increase of q^* indicates that the long period of PCL decreases with the incorporation of GO. Overall, these experimental results indicate that PCL undergoes significant structural changes with the incorporation of GO after leaving 50 days at room temperature.

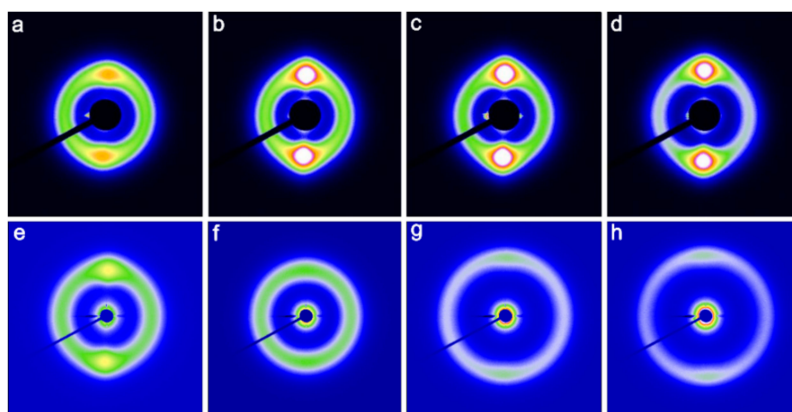


Figure 1. 2D-SAXS patterns of neat PCL and its nanocomposites: (a–d) 5 days; (e–h) 50 days. (a,e) Neat PCL; (b,f): PCL/GO-0.1; (c,g) PCL/GO-0.5; (d,h) PCL/GO-1.0.

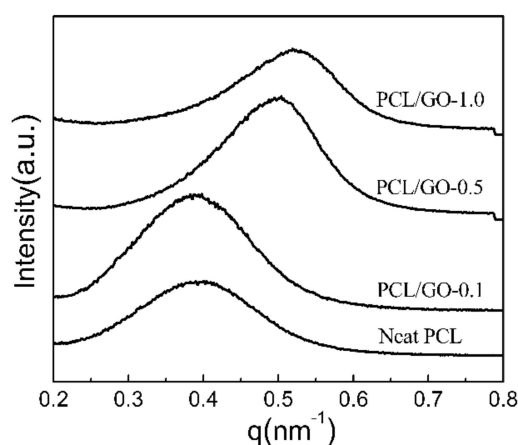


Figure 2. Radially integrated profiles of neat PCL and its nanocomposites collected from the corresponding 2D-SAXS patterns after leaving 50 days.

Further investigation was carried out using 2D-WAXD. Figure 3 shows 2D-WAXD patterns of neat PCL and its nanocomposites when they were kept 5 (a–d) and 50 (e–h) days after preparation. The influences of GO on the crystal structure and orientation can be estimated by comparing the 2D-WAXD patterns. From the patterns, two obvious isotropic diffraction circles corresponding to the (110) plane (inside) and the (200) plane (outside) of the PCL crystals are observed in all samples [12]. This result indicates that GO cannot influence the crystal structure and orientation of PCL crystals, and their variations with time cannot be observed directly from the patterns. Compared with the 2D-SAXS results, the orientation of PCL matrix is attributed to the fact that 2D layered GO could restrict the mobility of oriented PCL chains, and the orientation of PCL chains in amorphous parts can be kept in the cooling process. So the orientation signals observed in 2D-SAXS are contributed by the oriented chains in the amorphous parts.

In order to further investigate the variation of PCL crystal structure with time, WAXD curves of neat PCL and its nanocomposites are collected from the 2D-WAXD patterns (Figure 4). All samples present three typical diffraction peaks at $2\theta = 17.2^\circ$, 17.7° , and 19.1° , corresponding to (110), (111) and (200) crystal planes, respectively. However, the intensity of diffraction peaks obviously increases with increasing GO content, which means that the degree of crystallinity (X_c) of PCL matrix increases with the change of time. In addition, the more GO there is, the higher the X_c becomes. DSC measurements were employed to investigate the thermal effects of GO on PCL and their variations with time. Figure 5 shows DSC heating scans of neat PCL and its nanocomposites. For the samples left 5 days, both first and second heating scans show that the incorporation of GO cannot significantly affect the melting

temperature (T_m) of PCL matrix. After 50 days, first heating scans of samples show that PCL/GO nanocomposites exhibit higher T_m than Neat PCL, and the peaks become larger with the increase of GO content, which can certainly be attributed to a room temperature annealing process during sample storage. However, the second heating scans exhibit lower T_m for PCL/GO nanocomposites than Neat PCL, and the T_m values decrease with the increase of GO content. It has been reported that T_m is related to the crystalline thickness (L_c) of the polymer matrix, the thicker lamella has a higher melting temperature [36]. Thus, the decrease of T_m means the L_c of PCL matrix decreases with the incorporation of GO after erasing the heating history, and the more GO there is, the smaller the L_c is, which is caused by the degradation of the PCL matrix.

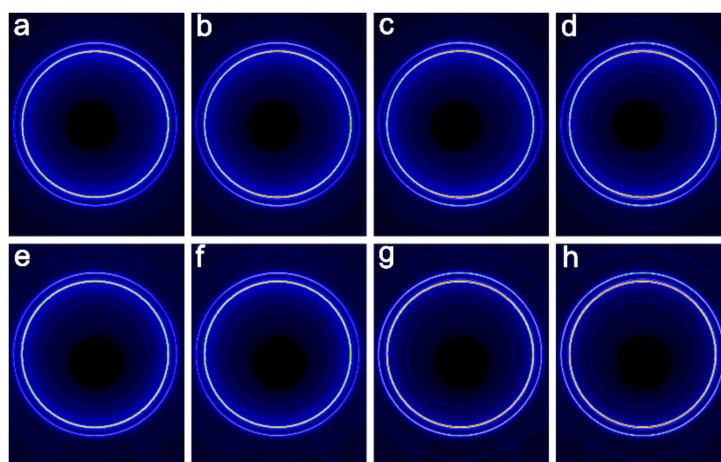


Figure 3. 2D-WAXD patterns of neat PCL and its nanocomposites: (a–d) 5 days; (e–h) 50 days. (a,e) Neat PCL; (b,f) PCL/GO-0.1; (c,g) PCL/GO-0.5; (d,h) PCL/GO-1.0.

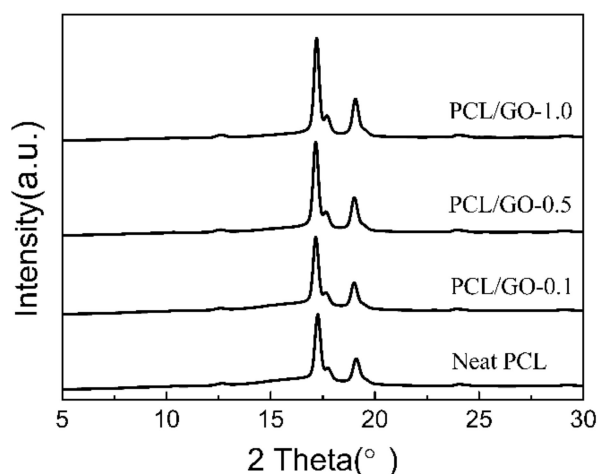


Figure 4. WAXD curves of neat PCL and its nanocomposites collected from the corresponding 2D-WAXD patterns after leaving 50 days.

The characteristic thermal data are listed in Table 1 to quantitatively investigate the effects of GO on PCL. The crystalline thickness L_c was calculated from long period and degree of crystallinity, $L_c = L \times X_c$, here X_c is obtained from the DSC results. 2D-SAXS results indicate that the long period of PCL matrix decreases with increasing GO content. However, WAXD and DSC results show that the degree of crystallinity increases with increasing GO content. The crystalline thickness calculated from these results slightly increases with the incorporation of GO, which corresponds to the change of T_m (first heating). These results indicate that the storage process cannot significantly affect the crystalline thickness of the PCL matrix. Meanwhile, these results imply that GO could induce the

degradation of PCL amorphous parts, resulting to the increase of X_c . This phenomenon has also been observed in the 2D-SAXS patterns. The decrease of T_m at second heating indicates that the molecular weight of the PCL matrix may most likely be reduced by degradation of amorphous part.

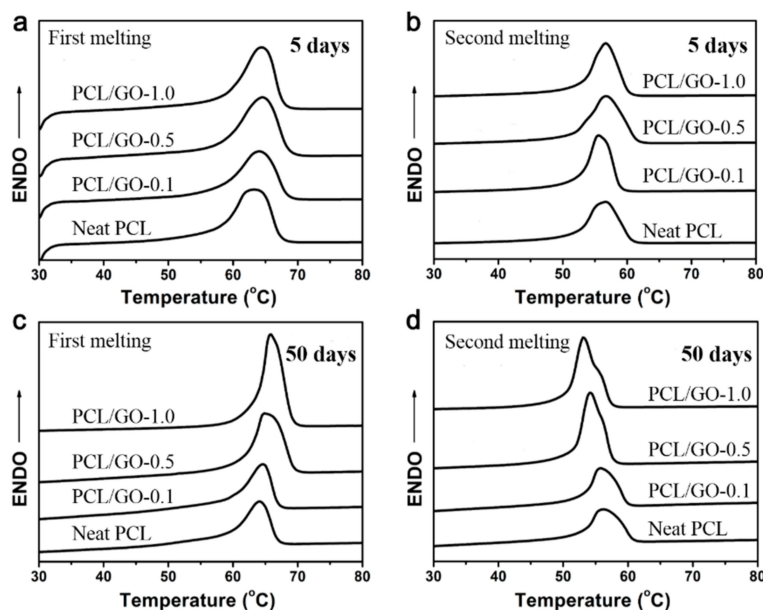


Figure 5. DSC curves of neat PCL and its nanocomposites.

Table 1. Thermal data obtained from the 2D-SAXS and DSC results of samples after leaving 50 days.

50 Days Sample	q^* (nm ⁻¹)	L (nm)	X_c (%)	L_c (nm)	T_m (°C) First Heating	T_m (°C) Second Heating
Neat PCL	0.392	16.02	68.8	11.02	64.1	56.2
PCL/GO-0.1	0.396	15.87	70.1	11.12	64.5	55.7
PCL/GO-0.5	0.499	12.59	90.0	11.33	65.6	54.1
PCL/GO-1.0	0.521	12.06	94.8	11.43	65.9	53.2

L is long period, q^* represents the peak position in the I - q curves, T_m is melting temperature, X_c represents degree of crystallinity and L_c represents crystalline thickness.

In order to confirm whether the structural change of PCL/GO nanocomposites is due to the change of PCL molecular weight, GPC was used to measure the molecular weight of PCL matrix with the incorporation of GO. Figure 6 shows the GPC curves of neat PCL and its nanocomposites after leaving for 50 days. The M_n calculated from these curves is 34,300, 30,300, 20,900 and 6200 g/mol for Neat PCL, PCL/GO-0.1, PCL/GO-0.5 and PCL/GO-1.0, respectively. These results indicate that the molecular weight of PCL matrix decreases with increasing GO content, which confirms that GO can induce the degradation of PCL chains during the storage process.

Overall, the above experimental results confirm that GO can influence the structure of the PCL matrix in the storage process, GO can induce the degradation of PCL chains in amorphous parts and has no obvious effects on crystalline parts, resulting that the X_c of PCL matrix increases with increasing GO content. The long period of polymer matrix contains a crystalline period and an amorphous period. In PCL/GO nanocomposites, the amorphous period was partly degraded in the storage process, which results in the decrease of the long period of PCL matrix. In addition, an isotropic growth of PCL crystals appeared during the cooling process, so 2D-WAXD results of PCL/GO nanocomposites could not show clear differences compared with Neat PCL bars. Previous studies proved that 2D layered GO could restrict the mobility of polyester chains, and the orientation of polymer chains in amorphous parts can be kept during the cooling process [9,12]. Thus, the orientation signals observed in 2D-SAXS are caused by the periodic structure of the oriented chains in the amorphous parts. In this study, GO could degrade the amorphous parts of PCL during the storage process, resulting in the

disappearance of scattering spots in the 2D-SAXS patterns (Figure 1e–h). After leaving for 50 days, the crystalline thickness slightly increased with increasing GO content, which is attributed to room temperature annealing and recrystallization processes. Moreover, the decrease of T_m in the second heating curves after leaving 50 days is caused by the degradation of PCL matrix.

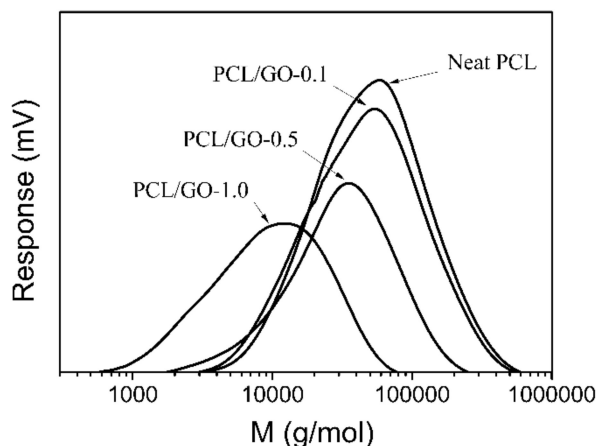


Figure 6. GPC curves of neat PCL and its nanocomposites after leaving 50 days.

In order to investigate the reason for the degradation of PCL, XPS was used to examine the surface properties of GO. Figure 7 shows the XPS spectra of GO. The signal peaks around 532 and 286 eV correspond to the O1s and C1s orbital electrons, respectively. As shown in Figure 7a, GO has a high degree of oxidation, indicating that large amounts of oxygen-containing functional groups were present on the surface of GO. Moreover, there were small amounts of N (1.4%), Cl (0.3%) and S (1.8%) elements present on the surface of GO (Figure 7b). In the chemical oxidation method to prepare GO, strong oxidizing agents such as sulfuric acid, potassium nitrate, potassium permanganate, hydrogen peroxide, hydrochloric acid are used to oxidize and treat graphite. In this study, GO was prepared with the standard treatment procedure, which was the same as the modified hummers' method, and strict post-treatment, including repeated centrifugation and dialysis, was employed to remove the strong acid. However, a small amount of N, Cl and S elements are still retained in the oxygen-containing functional groups, forming strong oxidative debris on the surface of GO. Moreover, this residual oxidative debris could interact with the ester groups in PCL chains, resulting in the degradation of the PCL matrix in the storage process. Furthermore, the content of residual oxygen-containing functional groups increases in proportion to the GO content; consequently, the degradation of PCL matrix in the storage process becomes more serious with increasing GO content.

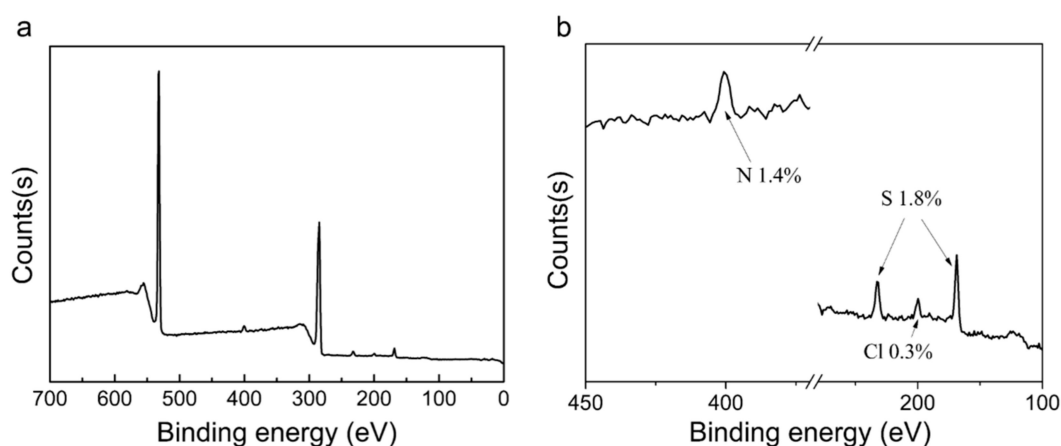


Figure 7. XPS spectra of GO.

4. Conclusions

The structural effects of residual groups of GO on the PCL/GO nanocomposites and their evolution with time have been investigated in detail. With the increase of storage time, the oxide groups on GO surface could degrade the amorphous parts of the PCL matrix. However, the increasing degree of crystallinity and almost constant crystalline thickness implies that oxidative degradation cannot degrade the crystal structure of the PCL matrix. The research is expected to be helpful in understanding the influence of residual groups of GO on the polyester matrix. To best use GO in the polymer nanocomposites, especially for polymers sensitive to acid, such as polyester, more optimized treatment should be adopted.

Author Contributions: Conceptualization, Z.W.; Methodology, Y.L.; Validation, H.X.; Formal Analysis, Y.L.; Investigation, T.D.; Data Curation, H.X.; Writing—Original Draft Preparation, T.D.; Writing—Review & Editing, Z.W., J.J.; Visualization, T.D.; Supervision, Z.W.

Funding: This research was funded by the National Natural Science Foundation of China (U1532114, 51773101), the National Key Research and Development Program of China (2017YFC1104800) and K. C. Wong Magna Fund in Ningbo University.

Acknowledgments: We thank Shanghai Synchrotron Radiation Facility (SSRF) for supporting the SAXS and WAXD test.

Conflicts of Interest: The authors declare no conflict of interest.

References

1. Veerapandian, M.; Lee, M.H.; Krishnamoorthy, K.; Yun, K. Synthesis, characterization and electrochemical properties of functionalized graphene oxide. *Carbon* **2012**, *50*, 4228–4238. [[CrossRef](#)]
2. Zhu, Y.W.; Murali, S.; Cai, W.W.; Li, X.S.; Suk, J.W.; Potts, J.R. Graphene and Graphene Oxide: Synthesis, Properties, and Applications. *Adv. Mater.* **2010**, *22*, 3906–3924. [[CrossRef](#)] [[PubMed](#)]
3. Hummers, W.S.; Offeman, R.E. Preparation of Graphitic Oxide. *J. Am. Chem. Soc.* **1958**, *80*, 1339. [[CrossRef](#)]
4. Staudenmaier, L. Verfahren zur Darstellung der Graphitsäure. *Ber. Dtsch. Chem. Ges.* **1898**, *31*, 1481–1487. [[CrossRef](#)]
5. Schniepp, H.C.; Li, J.L.; McAllister, M.J.; Sai, H.; Herrera-Alonso, M.; Adamson, D.H.; Prud'homme, R.K.; Car, R.; Saville, D.A.; Aksay, I.A. Functionalized Single Graphene Sheets Derived from Splitting Graphite Oxide. *J. Phys. Chem. B.* **2006**, *110*, 8535–8539. [[CrossRef](#)] [[PubMed](#)]
6. Kim, J.; Cote, L.J.; Huang, J. Two Dimensional Soft Material: New Faces of Graphene Oxide. *Acc. Chem. Res.* **2012**, *45*, 1356–1364. [[CrossRef](#)] [[PubMed](#)]
7. Xu, J.Z.; Liang, Y.Y.; Huang, H.D.; Zhong, G.J.; Lei, J.; Chen, C.; Li, Z.M. Isothermal and nonisothermal crystallization of isotactic polypropylene/graphene oxide nanosheet nanocomposites. *J. Polym. Res.* **2012**, *19*, 9975. [[CrossRef](#)]
8. Xu, J.Z.; Liang, Y.Y.; Zhong, G.J.; Li, H.L.; Chen, C.; Li, L.B.; Li, Z.M. Graphene Oxide Nanosheet Induced Intrachain Conformational Ordering in a Semicrystalline Polymer. *J. Phys. Chem. Lett.* **2012**, *3*, 530–535. [[CrossRef](#)] [[PubMed](#)]
9. Huang, H.D.; Xu, J.Z.; Fan, Y.; Xu, L.; Li, Z.M. Poly(L-lactic acid) crystallization in a confined space containing graphene oxide nanosheets. *J. Phys. Chem. B* **2013**, *117*, 10641–10651. [[CrossRef](#)] [[PubMed](#)]
10. Wang, G.S.; Wei, Z.Y.; Sang, L.; Chen, G.Y.; Zhang, W.X.; Dong, X.F.; Qi, M. Morphology, crystallization and mechanical properties of poly(ϵ -caprolactone)/graphene oxide nanocomposites. *Chin. J. Polym. Sci.* **2013**, *31*, 1148–1160. [[CrossRef](#)]
11. Hua, L.; Kai, W.; Inoue, Y. Synthesis and characterization of poly(ϵ -caprolactone)–graphite oxide composites. *J. Appl. Polym. Sci.* **2007**, *106*, 1880–1884. [[CrossRef](#)]
12. Wang, B.J.; Li, Y.G.; Weng, G.S.; Jiang, Z.Q.; Chen, P.; Wang, Z.B.; Gu, Q. Reduced graphene oxide enhances the crystallization and orientation of poly(ϵ -caprolactone). *Compos. Sci. Technol.* **2014**, *96*, 63–70. [[CrossRef](#)]
13. Wan, C.Y.; Chen, B.Q. Poly(ϵ -caprolactone)/graphene oxide biocomposites: Mechanical properties and bioactivity. *Biomed. Mater.* **2011**, *6*, 055010. [[CrossRef](#)] [[PubMed](#)]
14. Li, F.Y.; Yan, N.; Zhan, Y.H.; Fei, G.X.; Xia, H.S. Probing the reinforcing mechanism of graphene and graphene oxide in natural rubber. *J. Appl. Polym. Sci.* **2013**, *129*, 2342–2351. [[CrossRef](#)]

15. Zhan, Y.Q.; Yang, X.L.; Guo, H.; Yang, J.; Meng, F.B.; Liu, X.B. Cross-linkable nitrile functionalized graphene oxide/poly(arylene ether nitrile) nanocomposite films with high mechanical strength and thermal stability. *J. Mater. Chem.* **2012**, *22*, 5602–5608. [[CrossRef](#)]
16. Hu, J.M.; Jia, X.; Li, C.H.; Ma, Z.Y.; Zhang, G.X.; Sheng, W.B.; Zhang, X.L.; Wei, Z. Effect of interfacial interaction between graphene oxide derivatives and poly(vinyl chloride) upon the mechanical properties of their nanocomposites. *J. Mater. Sci.* **2014**, *49*, 2943–2951. [[CrossRef](#)]
17. Wan, Y.J.; Tang, L.C.; Gong, L.X.; Yan, D.; Li, Y.B.; Wu, L.B.; Jiang, J.X.; Lai, G.Q. Grafting of epoxy chains onto graphene oxide for epoxy composites with improved mechanical and thermal properties. *Carbon* **2014**, *69*, 467–480. [[CrossRef](#)]
18. Ma, W.S.; Li, J.; Zhao, X.S. Improving the thermal and mechanical properties of silicone polymer by incorporating functionalized graphene oxide. *J. Mater. Sci.* **2013**, *48*, 5287–5294. [[CrossRef](#)]
19. Li, Y.Q.; Pan, D.Y.; Chen, S.B.; Wang, Q.H.; Pan, G.Q.; Wang, T.M. In situ polymerization and mechanical, thermal properties of polyurethane/graphene oxide/epoxy nanocomposites. *Mater. Des.* **2013**, *47*, 850–856. [[CrossRef](#)]
20. Wang, X.W.; Zhang, C.A.; Wang, P.L.; Zhao, J.; Zhang, W.; Ji, J.H.; Hua, K.; Zhou, J.; Yang, X.B.; Li, X.P. Enhanced Performance of Biodegradable Poly(butylene succinate)/Graphene Oxide Nanocomposites via In Situ Polymerization. *Langmuir* **2012**, *28*, 7091–7095. [[CrossRef](#)] [[PubMed](#)]
21. Nawaz, K.; Khan, U.; Ul-Haq, H.; May, P.; O'Neill, A.; Coleman, J.N. Observation of mechanical percolation in functionalized graphene oxide/elastomer composites. *Carbon* **2012**, *50*, 4489–4494. [[CrossRef](#)]
22. Yun, Y.S.; Bae, Y.H.; Kim, D.H.; Lee, J.Y.; Chin, I.J.; Jin, H.J. Reinforcing effects of adding alkylated graphene oxide to polypropylene. *Carbon* **2011**, *49*, 3553–3559. [[CrossRef](#)]
23. Hua, L.; Kai, W.H.; Liang, Z.C.; Inoue, Y. Polyester/organo-graphite oxide composite: Effect of organically surface modified layered graphite on structure and physical properties of Poly(ϵ -caprolactone). *J. Polym. Sci. B Polym. Phys.* **2010**, *48*, 294–301. [[CrossRef](#)]
24. Cai, D.Y.; Song, M. A simple route to enhance the interface between graphite oxide nanoplatelets and a semi-crystalline polymer for stress transfer. *Nanotechnology* **2009**, *20*, 315708. [[CrossRef](#)] [[PubMed](#)]
25. Li, Z.L.; Young, R.J.; Kinloch, I.A. Interfacial Stress Transfer in Graphene Oxide Nanocomposites. *ACS Appl. Mater. Interface* **2013**, *5*, 456–463. [[CrossRef](#)] [[PubMed](#)]
26. Vallés, C.; Kinloch, I.A.; Young, R.J.; Wilson, N.R.; Rourke, J.P. Graphene oxide and base-washed graphene oxide as reinforcements in PMMA nanocomposites. *Compos. Sci. Technol.* **2013**, *88*, 158–164. [[CrossRef](#)]
27. Zhao, X.; Zhang, Q.H.; Hao, Y.P.; Li, Y.Z.; Fang, Y.; Chen, D.J. Alternate Multilayer Films of Poly(vinyl alcohol) and Exfoliated Graphene Oxide Fabricated via a Facial Layer-by-Layer Assembly. *Macromolecules* **2010**, *43*, 9411–9416. [[CrossRef](#)]
28. Wan, C.Y.; Chen, B.Q. Reinforcement and interphase of polymer/graphene oxide nanocomposites. *J. Mater. Chem.* **2012**, *22*, 3637–3646. [[CrossRef](#)]
29. Woodruff, M.A.; Huttmacher, D.W. The return of a forgotten polymer-Polycaprolactone in the 21st century. *Prog. Polym. Sci.* **2010**, *35*, 1217–1256. [[CrossRef](#)]
30. Chandra, R.; Rustgi, R. Biodegradable polymers. *Prog. Polym. Sci.* **1998**, *23*, 1273–1335. [[CrossRef](#)]
31. Wang, Y.; Li, Z.H.; Hu, D.H.; Lin, C.T.; Li, J.H.; Lin, Y.H. Aptamer/Graphene Oxide Nanocomplex for in Situ Molecular Probing in Living Cells. *J. Am. Chem. Soc.* **2010**, *132*, 9274–9276. [[CrossRef](#)] [[PubMed](#)]
32. Zhang, Y.J.; Hu, W.B.; Li, B.; Peng, C.; Fan, C.H.; Huang, Q. Synthesis of polymer-protected graphene by solvent-assisted thermal reduction process. *Nanotechnology* **2011**, *22*, 345601. [[CrossRef](#)] [[PubMed](#)]
33. Wang, B.J.; Li, H.Y.; Li, L.Z.; Chen, P.; Wang, Z.B.; Gu, Q. Electrostatic adsorption method for preparing electrically conducting ultrahigh molecular weight polyethylene/graphene nanosheets composites with a segregated network. *Compos. Sci. Technol.* **2013**, *89*, 180–185. [[CrossRef](#)]
34. Joly, S.; Garnaud, G.; Ollitrault, R.; Bokobza, L.; Mark, J.E. Organically Modified Layered Silicates as Reinforcing Fillers for Natural Rubber. *Chem. Mater.* **2002**, *14*, 4202–4208. [[CrossRef](#)]

35. Wang, B.J.; Zhang, Y.J.; Zhang, J.Q.; Gou, Q.T.; Wang, Z.B.; Chen, P.; Gu, Q. Crystallization behavior, thermal and mechanical properties of PHBV/graphene nanosheet composites. *Chin. J. Polym. Sci.* **2013**, *31*, 670–678. [[CrossRef](#)]
36. Wang, B.J.; Zhang, Y.J.; Zhang, J.Q.; Li, H.Y.; Chen, P.; Wang, Z.B.; Gu, Q. Noncovalent Method for Improving the Interaction between Reduced Graphene Oxide and Poly(ϵ -caprolactone). *Ind. Eng. Chem. Res.* **2013**, *52*, 15824–15828. [[CrossRef](#)]



© 2018 by the authors. Licensee MDPI, Basel, Switzerland. This article is an open access article distributed under the terms and conditions of the Creative Commons Attribution (CC BY) license (<http://creativecommons.org/licenses/by/4.0/>).